## 3.9 Interaction Region and Detector Backgrounds

### 3.9.1 Introduction

The design of the interaction region (IR) of the $e^+e^-$ collider involves an understanding of beam-beam effects, detector backgrounds, and the constraints required to maintain very small beam spot sizes at the interaction point (IP). Luminosity monitors with sufficient spatial and energy resolution can unfold the energy dependence of the beam-beam interaction's influence on the luminosity spectrum. With appropriate shielding around the IP a detector employing a high field solenoid and sufficiently granular tracking can be designed which is robust against backgrounds while allowing for excellent tracking and vertexing. Muon backgrounds in the detector are minimized by distancing the machine collimation system from the IP, introducing a 10 mrad bend between the linacs and final focus systems, and installing simple shielding magnets in the tunnel.

Ground motion from geologic and man-made sources must not move the final quadrupole doublet by an amount more than the vertical beam spot size. The rapid fall off of naturally occurring ground motion with increasing frequency, the use of precision beam position monitor based feedback loops sampling at the machine cycle frequency (120–180 Hz) to correct the beam orbits at low frequency, and the coherence arising from the interplay between the machine's optical lattice and the wavelength of a ground motion disturbance all conspire to make seismic motions in bedrock negligibly important to NLC luminosity. Quadrupole motion above the level of the bedrock, due to laboratory sources (pumps, etc.) or amplification of the driving term by its mechanical support within the detector, can be minimized by optically referencing the doublet to bedrock with a LIGO-style interferometer. Feedback signals can then drive either piezoelectric actuators or magnetic beam-corrector elements to reduce motion back down to naturally occurring seismic levels. The selection of a geologically quiet site, the design of the physical lab plant to minimize vibration, and the design of a robust final doublet support will all aid in controlling the ground motion problem.

### 3.9.2 Layout

In the schematic layout of Figure 3.3 the electron and positron linac arms are each followed by a 3.2-km-long collimation section and two final focus tunnels at $\pm 10$ mrad. These "Big Bends", 2.0 km from the interaction points (IP), protect the detectors from muons produced by the collimators, provide a 20 mrad crossing angle between incoming and outgoing beams, and allow for two experimental halls with IPs separated by 40 m. As trains consisting of 90 bunches of 0.65–1.1 $\times$ $10^{10}$ particles separated by 1.4 ns will collide at 120–180 Hz, a crossing angle is required so that a given bunch interacts with only its partner, and not with any other bunch still traveling to the IP.

Figure 3.31 shows a schematic of the masking and magnet layout in the interaction region. In the current final focus lattice the last quadrupole of the doublet (QFTA) ends 2 m from

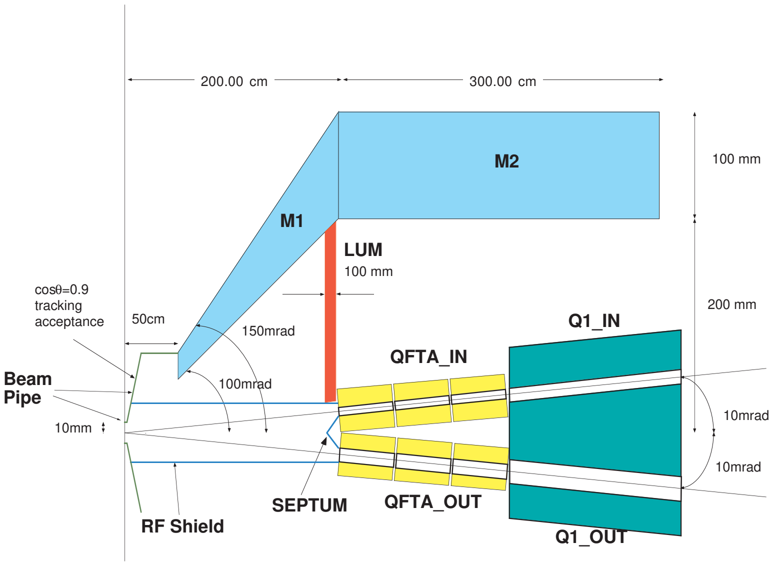


Figure 3.31: The interaction region masking and magnet layout.

the IP. Field strength and quality require that it be constructed of a machinable permanent magnetic material (samarium cobalt, for example). Its inner aperture radius is 4.5 mm and outer radius is 10.0 cm. A similar doublet with a 6 mm inner aperture radius to transport the outgoing disrupted beam, together with any synchrotron radiation and beamstrahlung photons, is symmetrically positioned horizontally across from QFTA. These two magnets are followed by a twin bore superconducting magnet to complete the doublet. Each is surrounded by a superconducting coil which shields the detector's solenoidal field.

A "dead cone", within which the vast majority of the low $p_t$, $e^+e^-$ pairs produced by the beam-beam interaction are confined, is defined by a conical tungsten mask which subtends the angular range from 100 to 150 mrad and 0.5 m$< z <$ 2 m. A cylindrical tungsten skirt, currently 10 cm thick, begins at $z$=2.0 m and $r$=20 cm. Its purpose is to protect any exterior detector from photons produced when the pair electrons and positrons strike the from face of the quadrupoles or luminosity monitor. The beam pipe is assumed at this time to have a radius of 1.0 cm for the first 2.5 cm from the IP. This will accommodate the inner layer of a vertex detector with acceptance out to $\cos\theta = 0.9$. The beam pipe then flares to a radius of 7.2 cm, switching from beryllium to 1-mm-thick stainless steel once it begins to follow the contour of the M1 mask. Within the beam pipe is a thin rf shield and septum which ease the transition from the narrow apertures of the input and exit quadrupoles to the beam pipe radius.

### 3.9.3 Backgrounds

The backgrounds anticipated at the NLC are each described in the following subsections. The experience of the SLD detector at SLC is that, when the accelerator is working well, all expected backgrounds are small. High luminosity correlates strongly with low backgrounds. While the calculations outlined below indicate that backgrounds will not be a substantial problem at the NLC, the prudent experimenter will design a detector which can handle the oft-occurring non-standard running conditions and *unexpected* backgrounds which are in the nature of linear colliders.

The background levels that can be supported require that we assume a detector model. Experience with the SLD's pixel vertex detector, based on 22 $\mu$m $\times$ 22 $\mu$m CCD pixels, is that hit density is the figure of merit. Integrating over its readout time of 19 bunch crossings, the SLD achieves 0.4 hits/mm$^2$ in its innermost layer. Tracks found in an 80 layer drift chamber are projected back to the vertex detector and hits lying within a three $\sigma$ extrapolation error window of roughly 1 mm are added to the track. The traditional figure of merit for vertex detector backgrounds is thus taken to be 1 hit/mm$^2$ per unit of time. Three to four layer self tracking silicon vertex detectors, with track extrapolation errors on the order of 10 $\mu$m, should be robust against backgrounds 10 to 20 times worse.

This section assumes that at the NLC the integration time for each detector is a train of 90 bunches. Depending on the technology actually used, this assumption may be overly pessimistic; nanosecond level timing and the ability to isolate background at the bunch level will certainly be a design goal for NLC detector components.

Raw occupancy is the figure of merit for a gas tracking chamber comprised of a relatively small number of wires each of which samples a large volume. The 5120 wire SLD chamber at $r = 20$ cm operates with 3–5% occupancy in good conditions. Simulations indicate that this is due to between one and ten thousand low energy photons produced from the secondary interactions of 2-MeV SR photons in the masking system. We take 1–10 thousand photons per train as the design goal for an NLC gas tracking chamber.

In SLD muons produced in the upstream collimators traverse the barrel calorimeter at the rate of one or two per beam crossing. In bad conditions there can be a factor of ten increase in the muon flux, at which point the schemes used to keep the muons from contributing to the trigger rate, and, to a lesser extent, the offline energy reconstruction offline, break down. The design goal of the muon protection system is that 1% of the beam can be scraped off in the collimation section and produce, on average, one muon per train of bunches that is transported into the detector.

### Muons

Figure 3.32 shows the results of the muon background simulation. The black diamonds show the ordinate is the number of muons that can interact in a given collimator and produce one muon in a 8 m by 8 m square detector. The abscissa is the location of the collimator in the tunnel. The points to the left between 4 and 5 km from the IP correspond to the collimation system; the points between 1 and 2 km from the IP correspond to locations where it is planned that the clean up collimators remove the slightest of beam tails. The uppermost of the two curves corresponds to the calculation when four 9 m long tunnel filling toroids are added to the final focus to intercept and deflect errant muons. One sees that this spoiler system added three orders of magnitude of protection and that we are two orders of magnitude within the design goal (which would correspond to roughly $10^{12}$). Without the spoilers we have a marginal situation. With or without spoilers, we are much more sensitive to beam particles lost in the FF after the big bend. Figure 3.32 shows that $10^6$ particles lost in the final focus, which is one part per million per train, will produce one muon that reaches the detector.

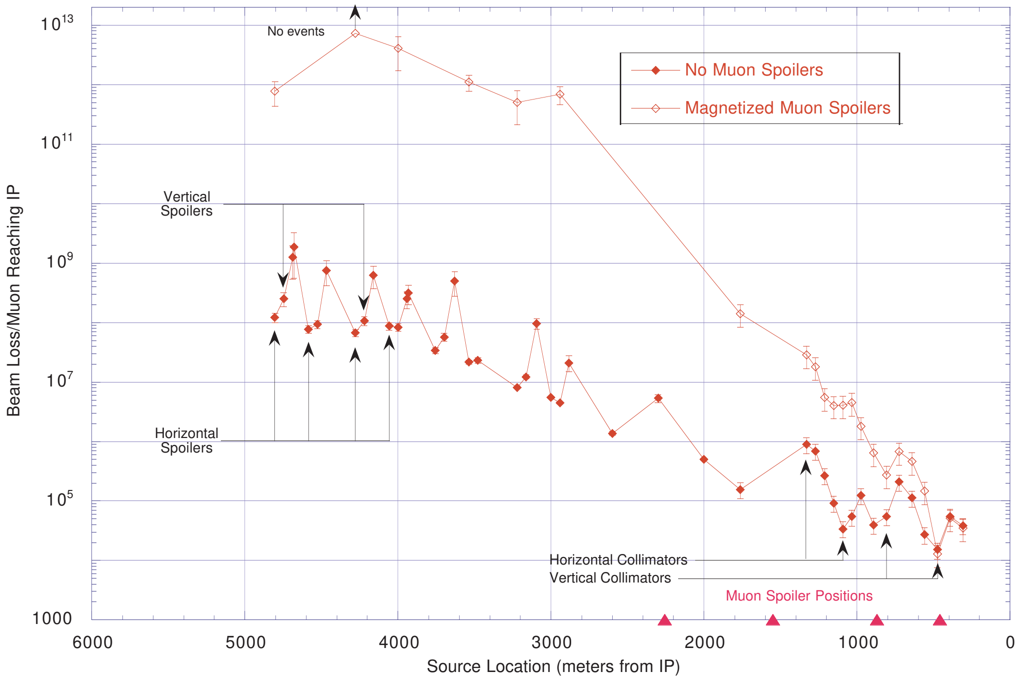


Figure 3.32: Muon backgrounds: the number of beam particles that can be lost on a given collimeter before producing one muon that strikes the detector.

### Pairs

Roughly $10^5$ pairs will be produced by the beam beam interaction each bunch crossing, predominately through the Bethe-Heitler interaction of beamstrahlung photons and electrons or positrons. For the most part the pairs are produced with low intrinsic $p_t$; the same sign partner will tend to be focused by the opposing beam while the opposite sign partner will be deflected outside the beam envelope by the magnetic field of the bunch. The finite beam dimensions then result in a very hard kinematic edge in the $p_t - \theta$ distribution (Figure 3.33).

By introducing a strong solenoidal magnetic field all particles with $p_t < 30$ MeV are curled up within the 5 cm minimum radius of the conical mask of Figure 3.31. All particles with $\theta$ less than the dead cone are curled up. The number of particles falling outside these two cuts is relatively small and manageable.

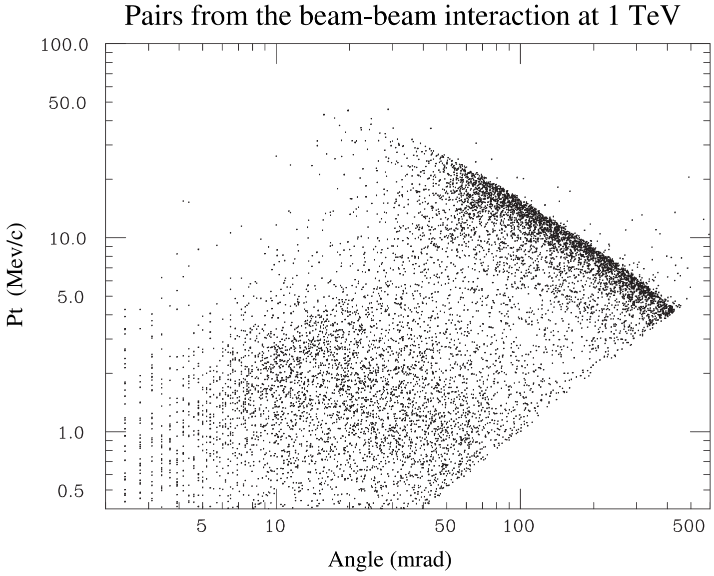


Figure 3.33: $p_t$ vs.$\theta$ distribution for pairs.

We have simulated the beam beam interaction at 1 TeV with the ABEL program. Figure 2.51 in the "Design of the NLC Detector" section of this document shows the hit density expected at $r = 2$ and 3 cm as a function of $z$ for a solenoidal field of 4 Tesla. At $r = 2$ cm, as long as our VXD lies within $z = 17$ cm, the hit density is manageable. Lowering the field would require that the innermost vertex layer be at correspondingly larger radius.

### Photons from Pairs

Pairs will interact with the beam pipe, inner vertex detector layers, rf shield septum, and front faces of the entrance and exit quads. As they interact, photons will be produced which will form a secondary background in the VXD and in any tracking chamber at larger radius.

To study this problem we have simulated the IR of Figure 3.31 with EGS4 using the 1-TeV ABEL ray files as input. Materials, thicknesses, and geometries have all been achieved at SLD. Figure 3.34 looks at the number of photons per train intercepting scoring planes with $\cos\theta = 0.90$ acceptance. Photon-to-hit conversion efficiencies are expected to be about the same for silicon tracking or gaseous drift chambers, a couple of percent. The hit densities are all well below $1/\mathrm{mm}^2$/train, even before taking into account conversion efficiency. However, the raw number of photons crossing the r=30 cm plane is rather large, approximately what we have taken as our figure of merit. The situation, as indicated in the figure, is made better by going to higher field. It is also possible that more innovative masking schemes will help. It does seem however that low granularity tracking devices will be marginal in the NLC background environment.

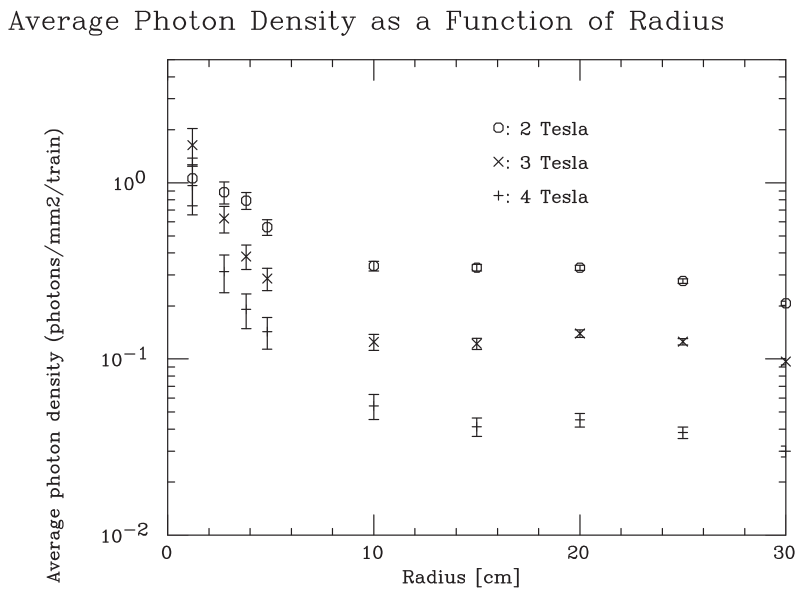


Figure 3.34: Photon hit density vs. radius.

### Synchrotron Radiation

SR produced by the core of the beam in the soft dipole bend just upstream of the final doublet and SR produced by particles at the edge of the phase space allowed by the collimation system can cause backgrounds in the detector. Most of the radiation escapes through the output quadrupole aperture; photons striking the inside of the incoming quadrupole aperture near its IP-side tip are the biggest problem. The soft bend SR from the core can be masked far from the IP. Figure 3.35 shows the energy distribution of SR from the beam tail as calculated for the 1 TeV lattice. As long as the QFTA aperture is large enough so that radiation produced immediately upstream in Q1 can escape the situation is not dramatic. If the QFTA aperture decreases below 4.3 mm radius or the tail collimation is loosened beyond $7\sigma_x$ and $35\sigma_y$ the energy deposited in the tip of QFTA increases dramatically.

Figure 3.36 shows the results of the EGS simulation using the SR energy distribution of Figure 3.35 as input. The charged particle hit density is tolerable for $r \geq 2$ cm and $B = 4$ Tesla, while the photon hit density is negligible in the region of the vertex detector. However, the photon density at 30 cm would correspond to having over 100,000 photons incident on a conventional drift chamber, a potentially worrisome figure were that technology chosen for the tracking system. Better masking, especially upstream in the lattice, and tighter collimation would reduce these numbers. Note also that the backgrounds would be much less for the 500 GeV lattice.

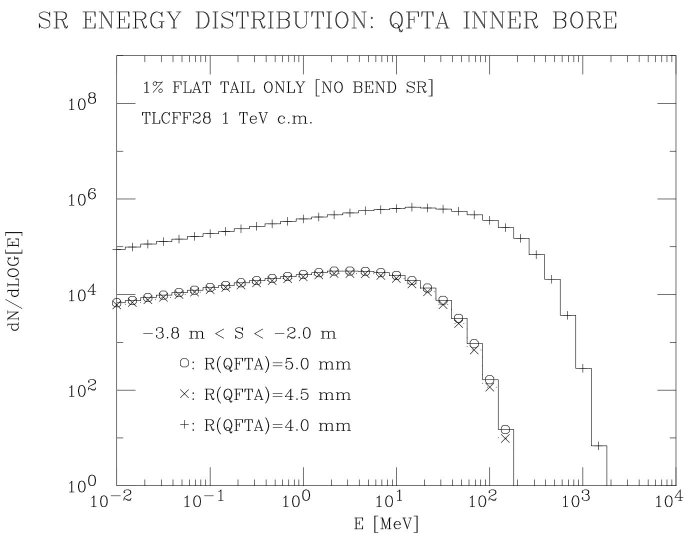


Figure 3.35: Synchrotron radiation energy distribution.

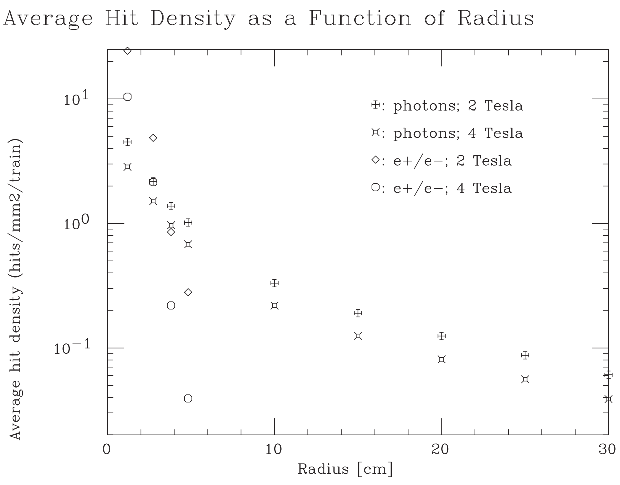


Figure 3.36: Synchrotron radiation hit distribution.

### 3.9.4 Quad Support and the Optical Anchor

As outlined in the introduction, the issue of ground motion was once thought to be a potential "show stopper" for a machine with nanometer sized beams. Our current understanding of the relationship between beam feedback, the ground motion spectrum, and the coherence resulting from the machine lattice and the wave nature of the ground motion is that by minimizing external sources of vibration and by firmly anchoring the final quadrupoles to bedrock luminosity will be preserved.

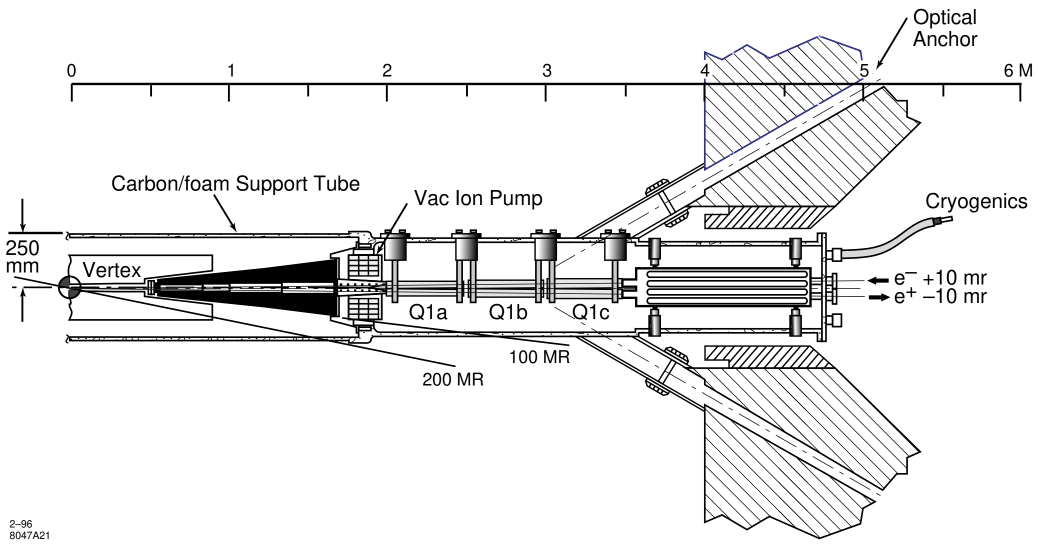


Figure 3.37: Current final doublet layout with 20-mrad crossing angle.

However, the final quads will need to be mounted inside a detector. Engineering the detector and the quad supports to avoid amplifying natural or cultural jitter sources is mandatory. Developing tools to remove the jitter that will nonetheless arise is highly prudent. Figure 3.37 shows an engineering drawing of our current ideas for the final quad layout and support.

In early tests at SLAC and DESY inertial seismometers driving pizeoelectric movers were used in feedback loops to inertially stabilize a magnet. A factor of three in amplitude reduction was achieved at each lab. Fears of using these devices within a particle detector magnetic field and a desire for larger reduction factors led to the search for optical solutions to the problem. The LIGO experiment, geophysicists, and astronomers have all addressed this problem through laser interferometry. The relative change in the length of two optical arms, $\ell_1$ and $\ell_2$, is related to an intensity change at a photodiode,

$$\frac{\delta I}{I} = \delta\Phi = 2\pi \cdot \frac{\delta(\ell_1 - \ell_2)}{\lambda}$$

For $\lambda = 633$ nm, and $\delta(\ell_1 - \ell_2) = 1$ nm, one will have $\delta\Phi = 0.02$ and this will cause a 2% intensity change on the photodiode.

While there are many constraints on the laser and optical system in this interferometer, including tolerances on the laser's intensity stability, frequency stability and power, as well as tolerances on pressure and temperature fluctuations in the optical transport arms, it appears that the solution is viable. Testing its performance and designing a detector which leaves room for optical lines of sight are what is required.

### 3.9.5 Conclusion

While more calculation and testing is required there does not appear to be any fundamental problem in designing an IR and detector which maintains the machine luminosity, can handle the backgrounds, and do the physics.